PNAS RESEARCH ARTICLE | NEUROSCIENCE OPEN ACCESS

Electrocalcium coupling in brain capillaries: Rapidly traveling electrical signals ignite local calcium signals

Amreen Mughal[a,1,2,3], Grant W. Hennig[a,1], Thomas Heppner[a], Nikolaos M. Tsoukias[b], David Hill-Eubanks[a], and Mark T. Nelson[a,c,2]

Affiliations are included on p. 10.

Contributed by Mark T. Nelson; received July 26, 2024; accepted November 15, 2024; reviewed by Jessica A. Filosa and Manuel F. Navedo

The routing of blood flow throughout the brain vasculature is precisely controlled by mechanisms that serve to maintain a fine balance between local neuronal demands and vascular supply of nutrients. We recently identified two capillary endothelial cell (cEC)-based mechanisms that control cerebral blood flow in vivo: 1) electrical signaling, mediated by extracellular K^+-dependent activation of strong inward rectifying K^+ (Kir2.1) channels, which are steeply activated by hyperpolarization and thus are capable of cell-to-cell propagation, and 2) calcium (Ca^{2+}) signaling, which reflects release of Ca^{2+} via the inositol 1,4,5-trisphosphate receptor (IP_3R)—a target of G_q-protein-coupled receptor signaling. Notably, Ca^{2+} signals were restricted to the cell in which they were initiated. Unexpectedly, we found that these two mechanisms, which were presumed to operate in distinct spatiotemporal realms, are linked such that Kir2.1-dependent hyperpolarization induces increases in the electrical driving force for Ca^{2+} entry into cECs through resident TRPV4 channels. This process, termed electrocalcium (E-Ca) coupling, enhances IP_3R-mediated Ca^{2+} release via a Ca^{2+}-induced Ca^{2+}-release mechanism, and allows focally induced hyperpolarization, including that initiated by ATP-dependent K^+ (K_{ATP}) channels, to travel cell-to-cell via activation of Kir2.1 channels in adjacent cells, providing a mechanism for the "pseudopropagation" of Ca^{2+} signals. Computational modeling supported the basic features of E-Ca coupling and provided insight into the intracellular processes involved. Collectively, these data provide strong support for the concept of E-Ca coupling and provide a mechanism for the spatiotemporal integration of diverse signaling pathways in the control of cerebral blood flow.

blood flow | brain capillaries | endothelial cells | calcium signaling | potassium channels

Significance

This study describes an unexpected linkage between two neurovascular coupling mechanisms with different spatiotemporal characteristics—electrical signaling (long range and rapid) and Ca^{2+} signaling (slower and localized)—that operate in brain capillary endothelial cells (cECs). This linkage, termed electrocalcium (E-Ca) coupling, reflects electrical (hyperpolarization)-induced increases in the driving force for Ca^{2+} entry into cECs produced by activation of cEC K^+ channels (Kir2.1 or K_{ATP}). This process repeats in successive cells owing to activation of Kir2.1 channels by hyperpolarization, a unique property of these channels. This process, which can be conceptualized as a rapidly traveling electrical (hyperpolarizing) wave that ignites a trail of "embers"—Ca^{2+} signals—in its wake, provides a mechanism for "pseudopropagation" of Ca^{2+} signals.

Neurons in the brain have a limited capacity for storage of energy substrates and thus rely on a just-in-time delivery system that links increases in neuronal activity to increases in the local delivery of blood-borne nutrients. This neurovascular coupling (NVC) process, mediated by a number of mechanisms, underlies the activity-dependent increases in tissue perfusion (functional hyperemia) responsible for supporting ongoing and dynamic changes in neuronal activity. Our studies on NVC have established that strong inward rectifying K^+ (Kir2.1) channels in capillary ECs (cECs) are central players in a key mechanism underlying functional hyperemic responses in the barrel cortex (1). These channels are activated by modest elevations in perivascular K^+, released into the extracellular space by neurons as a byproduct of each action potential. Because these channels are also steeply activated by hyperpolarization and are expressed in all cECs, the hyperpolarization they produce can spread rapidly to neighboring cECs, producing a propagating electrical current that ultimately reaches upstream arterioles and arteries, relaxing surrounding, electrically coupled contractile pericytes enroute (2). At the arterial/arteriolar level, it hyperpolarizes smooth muscle cells (SMCs), causing vasodilation and an increase in blood flow along the vascular path leading to the site of signal initiation (1). Accordingly, in addition to its conduit function, the vast network of brain capillaries, which positions cECs in close apposition to every neuron, acts as a sensory web that detects local neural activity and translates this information into a local hyperemic response, thus playing a central role in the NVC process.

Against this backdrop, we recently discovered that ongoing neuronal activity in the brain produces an astonishing array of Ca^{2+} signals in brain cECs in vivo. These signals occur at high frequency (3,000 to 6,000 events/minute/μL of the cortex) and exhibit a broad range of durations (<2 s to ~60 s) and Ca^{2+} output (range, ~4 orders of magnitude). These local Ca^{2+} transients are dependent on neuronal activity and reflect the activation of cEC G_q-type G protein-coupled receptors (G_qPCRs) by neuronally derived ligands. Activated G_qPCRs, in turn, signal through phospholipase C (PLC) to hydrolyze the plasma membrane phospholipid, phosphatidylinositol 4,5-bisphosphate (PIP_2) to

[1]A.M. and G.W.H. contributed equally to this work.

[2]To whom correspondence may be addressed. Email: Amreen.mughal@nih.gov or Mark.Nelson@uvm.edu.

[3]Present address: The Neurovascular Research Unit, Stroke Branch-National Institute of Neurological Disorders and Stroke, Translational Vascular Medicine Branch-National Heart, Lung, and Blood Institute, NIH Intramural Research, Bethesda, MD 20892.

This article contains supporting information online at https://www.pnas.org/lookup/suppl/doi:10.1073/pnas.2415047121/-/DCSupplemental.

Published December 11, 2024.

diacylglycerol and inositol 1,4,5-trisphosphate (IP_3), the latter of which promotes the release of $Ca^{2+}$from intracellular stores via IP_3 receptors (IP_3Rs) in the endoplasmic reticulum (ER) membrane. The resulting increases in intracellular Ca^{2+} activate Ca^{2+}-dependent endothelial nitric oxide synthase (eNOS), increasing the local production and release of nitric oxide (NO), which dilates contractile pericytes in an arteriole-proximate region of the capillary bed termed the arteriole-capillary transition (ACT) zone (3, 4), providing a mechanism for the fine regulation of blood flow within the capillary bed (5). Notably, we found that these local Ca^{2+} signals are restricted to individual cECs and do not spread between cECs (5).

This setup, with rapid electrical signaling mechanisms capable of acting over long distances and relatively slow cEC Ca^{2+} signaling presumably acting locally to regulate blood delivery within the capillary network, would suggest that electrical and Ca^{2+} signaling mechanisms operate in two very different spatiotemporal domains. However, electrical signaling in the form of passing waves of hyperpolarization can significantly increase the driving force for Ca^{2+} entry by imposing a steeper, more favorable electrochemical gradient in the cECs through which Ca^{2+} ions pass. This would increase Ca^{2+} influx and modulate Ca^{2+} activity in these cells, effectively linking electrical and Ca^{2+} signaling.

Key elements in this linkage are cEC membrane cation channels, which provide a conduit for hyperpolarization-enhanced Ca^{2+} entry. Prominent among the cation channels expressed in cECs are TRPV4 (transient receptor potential vanilloid 4) channels. Not only do these nonselective cation (NSC) channels conduct Ca^{2+} influx into cECs in response to hyperpolarization, they are also activated by G_qPCR signaling, which disinhibits these channels by depleting PIP_2—an inhibitor of TRPV4 channel activity (5–7). Thus, membrane hyperpolarization propagated by cell-to-cell activation of Kir2.1 channels, acting in conjunction with G_qPCR signaling in individual cECs, converges on TRPV4 channels to form a molecular module that drives Ca^{2+} signaling in cECs through an IP_3R-mediated, Ca^{2+}-induced Ca^{2+}-release (CICR) mechanism. In addition to Kir2.1 channels, ATP-dependent K^+ (K_{ATP}) channels are also prominently expressed in cECs and can contribute to cEC hyperpolarization (8). Notably, K_{ATP} channels are activated by G_s-subtype–dependent GPCR (G_sPCR) signaling through stimulation of adenylyl cyclase (AC)-mediated production of cAMP and subsequent activation of cAMP-dependent kinase (PKA), which activates K_{ATP} channels (8–12). Consistent with this, we recently showed that the G_sPCR ligands, adenosine and calcitonin gene-related peptide (CGRP), can activate K_{ATP} channels and hyperpolarize cECs and pericytes, resulting in a significant increase in cerebral blood flow (CBF) (8).

In this study, we explored the linkage between changes in cEC membrane potential and Ca^{2+} signaling, here termed E-Ca coupling, specifically examining in detail how the increased driving force for Ca^{2+} entry in cECs via TRPV4 channels resulting from Kir2.1 (or K_{ATP}) channel activation-dependent membrane hyperpolarization promotes Ca^{2+} signals by enhancing IP_3R-dependent CICR. We further investigated the role of Kir2.1 channels as facilitators of long-distance Ca^{2+} signaling and targets of G_sPCR-K_{ATP} channel signaling. Collectively, our findings suggest that, as hyperpolarization propagates along a microvascular path, it creates conditions conducive to Ca^{2+} influx in cECs through which it passes, facilitating Ca^{2+} signaling in cECs at a distance from the stimulus site. Our findings also provide a framework for understanding how G_s- and G_qPCR signaling intersect with hyperpolarizing mechanisms to contribute to the richness of local and long-distance Ca^{2+} signals throughout the capillary network.

Results

Kir2.1-Dependent Hyperpolarizing Waves Drive Ca^{2+} Signals in Their Wake via E-Ca Coupling. In our previous paper, we speculated that electrical (hyperpolarizing) signaling (mediated by Kir2.1 channels) and Ca^{2+} signaling (reflecting IP_3R-mediated release of Ca^{2+} from intracellular stores) intersect in central nervous system (CNS) cECs such that hyperpolarization increases the driving force for Ca^{2+} influx, resulting in an increase in Ca^{2+} signals (5).

To first confirm that activation of Kir2.1 channels causes sufficient hyperpolarization of CNS cECs to produce a relevant increase in the driving force for Ca^{2+} entry, we quantified the changes in membrane potential that accompany activation of Kir2.1 channels using microelectrodes. We focused on cECs within the ACT zone (3/4th-order branch), based on its unique functional role in the CNS microvasculature (2–4, 13). For these experiments, we used an ex vivo, whole-mount, pressurized, retina preparation in which the entire retina tissue is pinned down en face and the ophthalmic artery is cannulated and perfused (8, 14). The advantages of using the retina—an extension of the CNS—is that the resulting ex vivo preparation provides a planar view of the superficial vasculature and allows easy access to cells of interest for impalement (Fig. 1*A*). Appropriate target cell impalement was confirmed by monitoring the fluorescence of iFluor 488-conjugated hydrazide that diffused from dye-filled microelectrodes into the cEC (Fig. 1*A*). We found that bath perfusion of the retina preparation with 10 mM K^+, a concentration within the optimal range for Kir2.1 channel-mediated hyperpolarization (15), and consistent with elevations in extracellular K^+ that accompany neuronal action potentials (16), hyperpolarized the membrane potential in cECs to −57 ± 4 mV from a resting membrane potential of −29 ± 3 mV. The Goldman–Hodgkin–Katz (GHK) equation predicts that hyperpolarizing the membrane potential to this extent would increase the driving force for Ca^{2+} entry into cECs by 76% (assuming Ca^{2+}_o = 2 mM, Ca^{2+}_i = 100 nM, and constant permeability), indicating that activation of Kir2.1 channels is capable of strongly increasing Ca^{2+} influx into the cell. The hyperpolarizing effect 10 mM K^+ was inhibited by bath application of Ba^{2+}, a selective blocker of Kir2 channels (17–19) at the concentration used (100 μM) (Fig. 1 *B* and *C*).

We previously reported that tetrodotoxin (TTX; 3 μM) and Ba^{2+} (100 μM), applied individually, eliminate ~70 to 80% of baseline Ca^{2+} signals in the barrel cortex, suggesting that these signals are largely dependent on ongoing neuronal activity and Kir channel function (5). To confirm that cEC Kir2.1 channels are specifically responsible for the generation of these Ca^{2+} signals, we developed a tamoxifen-inducible, EC-specific Kir2.1-knockout (KO) mouse (*Cdh5*-Cre^{ERT2}; $Kir2.1^{fl/fl}$; hereafter, EC Kir2.1-KO mice), crossed with *Cdh5*-GCaMP8 mice expressing the Ca^{2+} biosensor, GCaMP8. Anesthetized mice carrying the appropriate genetic elements (*Materials and Methods*) were fitted with a cranial window, and Ca^{2+} signals in cECs were subsequently examined in layer II/III of the barrel cortex using 2-photon laser-scanning fluorescence microscopy. Using a refinement of our original analytical approach (*Materials and Methods*), we found that ~70% of ongoing (baseline) Ca^{2+} signals in a 425 × 425 μm field of view (FOV) were eliminated in mice lacking Kir2.1 channels in ECs (Fig. 1 *D* and *E* and Movie S1). These results, which are virtually identical to those obtained previously using Ba^{2+} and reanalyzed here (*SI Appendix*, Fig. S1 *A* and *B* and Movie S2), confirm a central role for cEC Kir2.1 channels in the neuronal activity-dependent generation of cEC Ca^{2+} signals and establish the basic features of E-Ca coupling.

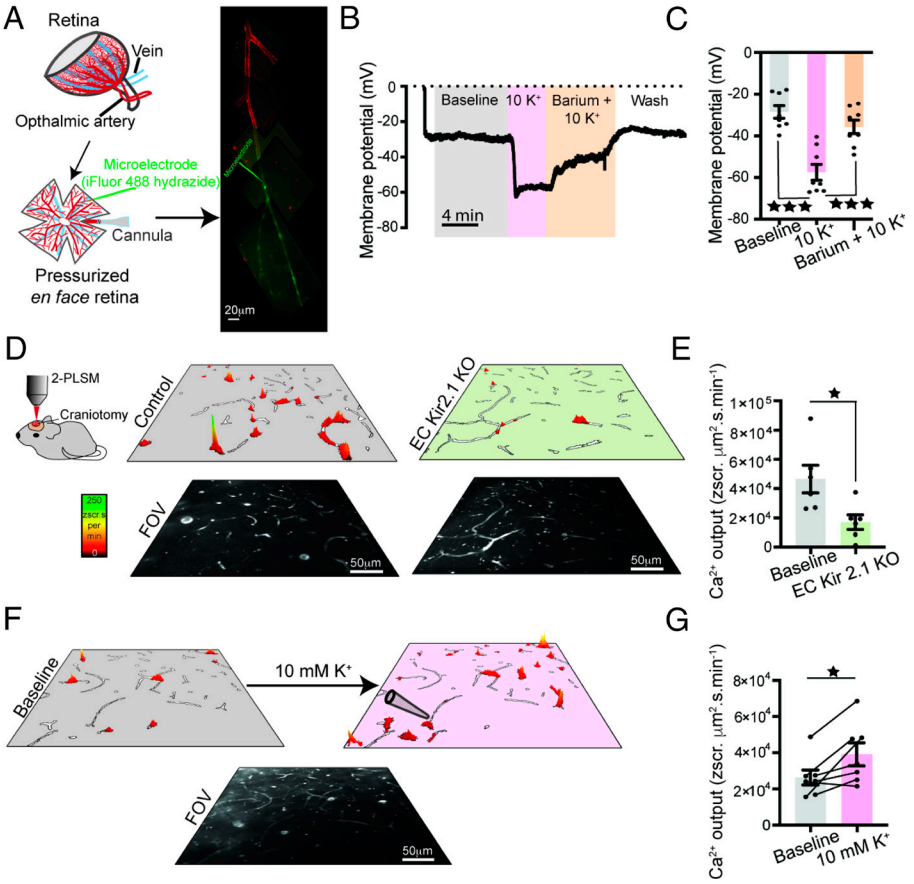

Fig. 1. Spreading hyperpolarization induced by stimulation of cEC Kir2.1 channels drives pseudopropagation of Ca^{2+} signals. (*A*) *Left*: Graphical representation of an en face pressurized retina preparation. *Right*: Image of the retinal vasculature labeled with rhodamine-isolectin (red) to stain the internal elastic lamina and show the transition from arteriole to capillaries; also depicted is a microelectrode filled with Alexa 488-hydrazide (green) showing dye diffusion through coupled cECs. (*B* and *C*) Original tracing (*B*) and summary data (*C*) showing changes in membrane potential in retina cECs from wild-type mice following bath application of 10 mM K^+, with and without Ba^{2+} (100 μM), obtained using sharp electrodes (n = 8 experiments, 8 mice; ***$P < 0.0001$, one-way ANOVA with Tukey's multiple comparisons test). (*D*) Graphical representation of in vivo imaging setup and representative maps showing prevalence of Ca^{2+} events in cECs in control (*Left*) and EC Kir2.1-KO (*Right*) mice. *Top* panels: prevalence maps; *Bottom* panels: imaging FOV (425 × 425 μm). (*E*) Summary data showing Ca^{2+} activity for control and EC Kir2.1-KO mice (n = 6 experiments, 6 mice; *$P < 0.05$, unpaired *t* test). (*F* and *G*) Prevalence maps (*F*) and summary data (*G*) showing cEC Ca^{2+} activity before and after picospritzing 10 mM K^+ onto 3rd/4th-order capillaries (n = 7 experiments, 7 mice; *$P < 0.05$, paired *t* test).

To directly assess E-Ca coupling in response to a defined, acute neuronal stimulus rather than to ongoing neuronal activity of indeterminate origin, we focally activated cEC Kir2.1 channels by picospritzing 10 mM K^+ (mimicking neuronal activity) adjacent to an ACT zone capillary segment using a picrospritzer micropipette. We then measured cEC Ca^{2+} responses in the entire FOV at ~2.5 Hz for 236 s. Localized application of 10 mM K^+ increased cEC Ca^{2+} responses by ~35% within the 425 × 425 μm FOV (Fig. 1 *F* and *G* and Movie S3). Taken together with results obtained under basal conditions in EC Kir2.1-KO mice, these findings support the concept that hyperpolarizing signals transmitted by cECs evoke Ca^{2+} signals at various points along the transmission path. This provides a mechanism for increasing the frequency of local Ca^{2+} signals at distances from the original stimulus site that we have dubbed "pseudopropagation," reflecting its passing resemblance to cell-to-cell conduction of Ca^{2+} signals and potential to exert impacts at a distance from the stimulus site.

To better appreciate the distances and directions over which hyperpolarizing signals spread through capillary networks, we examined arteriole-to-venule distances through capillary beds and capillary branching patterns (Fig. 2 and Movie S4). Distance measurements were performed on 3D models of the cortical vasculature and distances were measured as "vessel distance"—involving tracking through vessels until a particular point was reached. The average 3D distance between capillary branch points was 31.7 μm (Fig. 2 *A* and *B*), a value in reasonable agreement with our previous calculations (35.6 μm) and the length of an individual EC (34.9 μm) (see ref. 5). The median distance between arterioles and venules obtained using a 3D flood-fill approach (*Materials and Methods*) was 263.8 μm, encompassing ~8 ECs (Fig. 2*C*). These values are comparable to those reported in a previous rigorous brain microvasculature analysis by Kleinfeld et al. which estimated 6 to 8 branches from arteriole to venule (20).

We next examined the directionality of hyperpolarization spread to determine whether there was any inherent bias for hyperpolarizing signals to travel toward arterioles, as might be expected based on the common conceptualization of NVC mechanisms as promoting upstream (i.e., arteriolar) dilation. If this were the case, disproportionally more Ca^{2+} signals should be observed toward the arteriolar side of capillary beds, particularly in the primary branch of the transition zone, where there is only one route available for hyperpolarizing signals to reach an arteriole. Our analysis showed that Ca^{2+} signals were equally distributed on the arteriolar and venule side of capillary beds, with the highest density of Ca^{2+} signals detected at ~200 μm from the nearest major vessel (Fig. 2 *D* and *E*)—the midpoint of the capillary bed between arteriolar and venule sides where the number of branches is maximum. This lack of detectable directional bias in cEC Ca^{2+} events toward arterioles or venules implies that Kir2.1-mediated hyperpolarizing signals propagate in all directions following direct

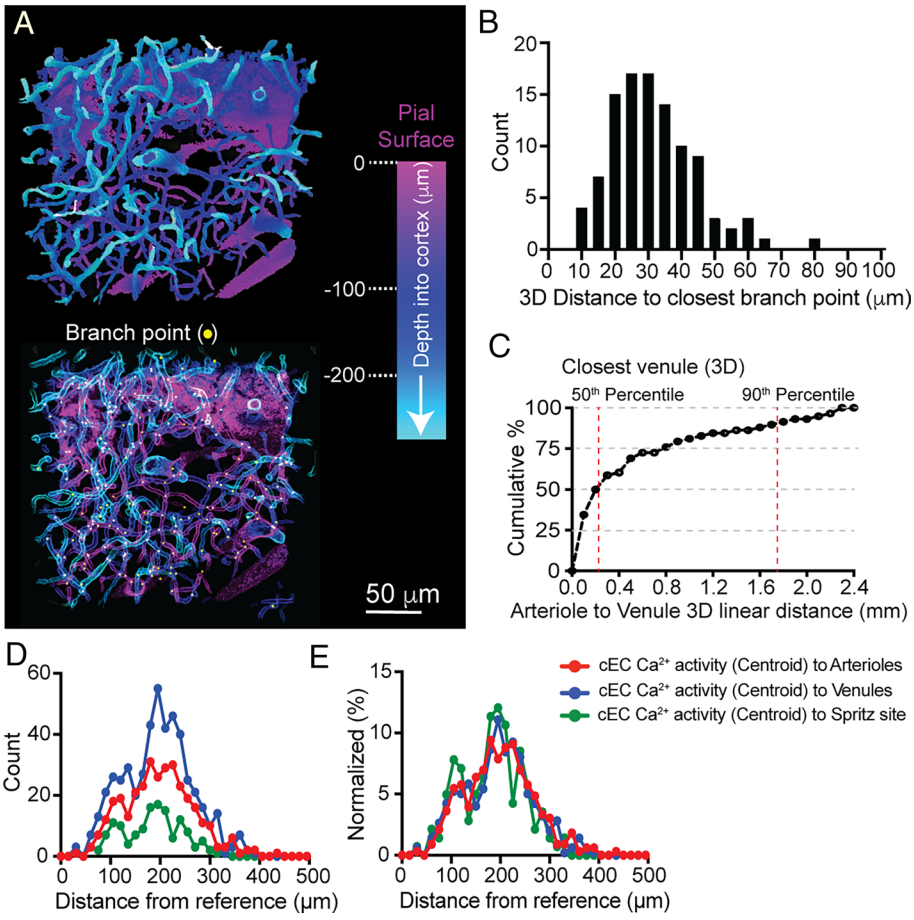

Fig. 2. Structure and density analysis of capillary beds in the somatosensory cortex. (*A*) Example of an "inside out" view of blood vessels in the outermost layers of the mouse somatosensory cortex. *Top* panel: Depth of vessels, color-coded from deepest (cyan) to shallowest (magenta). From this perspective, large diameter pial vessels on the brain surface (magenta) lie behind foreground (deeper) vessels; a PA is visible in the center of the volume. *Bottom* panel: Locations of vessel branch points (yellow spheres). (*B*) Histogram showing average 3D distance between closest branch points. Distance calculated in the middle half of the imaging volume was 31.72 ± 12.84 μm (n = 104; ~4,800 branch points/mm^3). (*C*) 3D linear distance from each arteriole to all venules, determined using a 3D flood-fill algorithm. Median distance from an arteriole to the closest venule was 263.8 μm (n = 59 measurement pairs). Data are from 72 arterioles and 98 venules in 26 FOVs from 16 mice. (*D* and *E*) Raw (*D*) and normalized (*E*) data showing distance of Ca^{2+} events from arterioles (red), venules (green), and spritz site. The large number of Ca^{2+} events is observed at the average mid region of multiple capillary beds (~200 μm), where diverging branches transition to converging branches, indicative of unbiased (i.e., omnidirectional) spread of the hyperpolarizing wave following focal stimulation.

focal stimulation of the microvasculature rather than favoring an arteriolar path.

K_{ATP}-Channel-Dependent Hyperpolarization Intersects with the Kir2.1-Dependent E-Ca Coupling Mechanism to Evoke Long-Distance Ca^{2+} Signals. Although the biophysical properties of the Kir2.1 channel make it uniquely suited to sense extracellular K^+ changes/neuronal activity and hyperpolarize cECs, it is not the only ion channel expressed in these cells capable of exerting a hyperpolarizing influence; K_{ATP} channels are also present in these cells (8). In this previous study, we reported that activation of K_{ATP} channels with the synthetic opener, pinacidil (10 μM), robustly hyperpolarized the membrane potential, shifting it from approximately −30 mV to −80 mV. This ~50-mV hyperpolarization would be predicted to increase Ca^{2+} influx by ~150%, based on the GHK equation.

To determine whether K_{ATP} channel-mediated hyperpolarization, like Kir2.1-mediated hyperpolarization, drives Ca^{2+} signaling in vivo, we first used 2-photon laser-scanning fluorescence microscopy to examine ongoing (baseline) Ca^{2+} signals in the barrel cortex of cranial window model *Cdh5*-GCaMP8 mice, testing the effects of glibenclamide, a selective synthetic K_{ATP} channel inhibitor. Glibenclamide (10 μM) significantly attenuated baseline cEC Ca^{2+} events, reducing them by ~50% (Fig. 3 *A* and *B* and Movie S5). We have found that cAMP-dependent protein kinase (PKA) is the primary activator of K_{ATP} channels in vascular cells (e.g., SMCs, pericytes, ECs), reflecting the stimulation of AC and production of cAMP following activation of G_sPCRs by agonists such as adenosine and CGRP (8, 9, 21). Accordingly, we tested the effect of blocking K_{ATP} channel activation on Ca^{2+} signaling in *Cdh5*-GCaMP8 mice by inhibiting upstream AC activity with SQ22536 (300 μM). This maneuver dramatically decreased Ca^{2+} signals (by ~80%) (Fig. 3 *C* and *D*), suggesting that G_sPCR agonists released as a consequence of local neural activity drive cEC Ca^{2+} signals via K_{ATP}-dependent hyperpolarization. Collectively, these observations indicate that cEC K_{ATP} channels exert a strong influence on baseline cEC Ca^{2+} signaling.

We next measured cEC Ca^{2+} signals in vivo in response to focal stimulation of cEC K_{ATP} channels with pinacidil (10 μM). Picospritzing pinacidil around ACT zone capillary branches caused an increase in cEC Ca^{2+} signaling throughout the FOV that propagated bidirectionally toward arterioles and venules from the site of stimulation (Fig. 3 *E* and *F* and Movie S6), similar to Kir2.1-mediated signaling. Focal stimulation of K_{ATP} channels induced approximately a 50% increase in Ca^{2+} signals in the FOV. Taken together, these results indicate that local activation of K_{ATP} channels generates Ca^{2+} signals throughout the FOV, suggesting propagating membrane hyperpolarization.

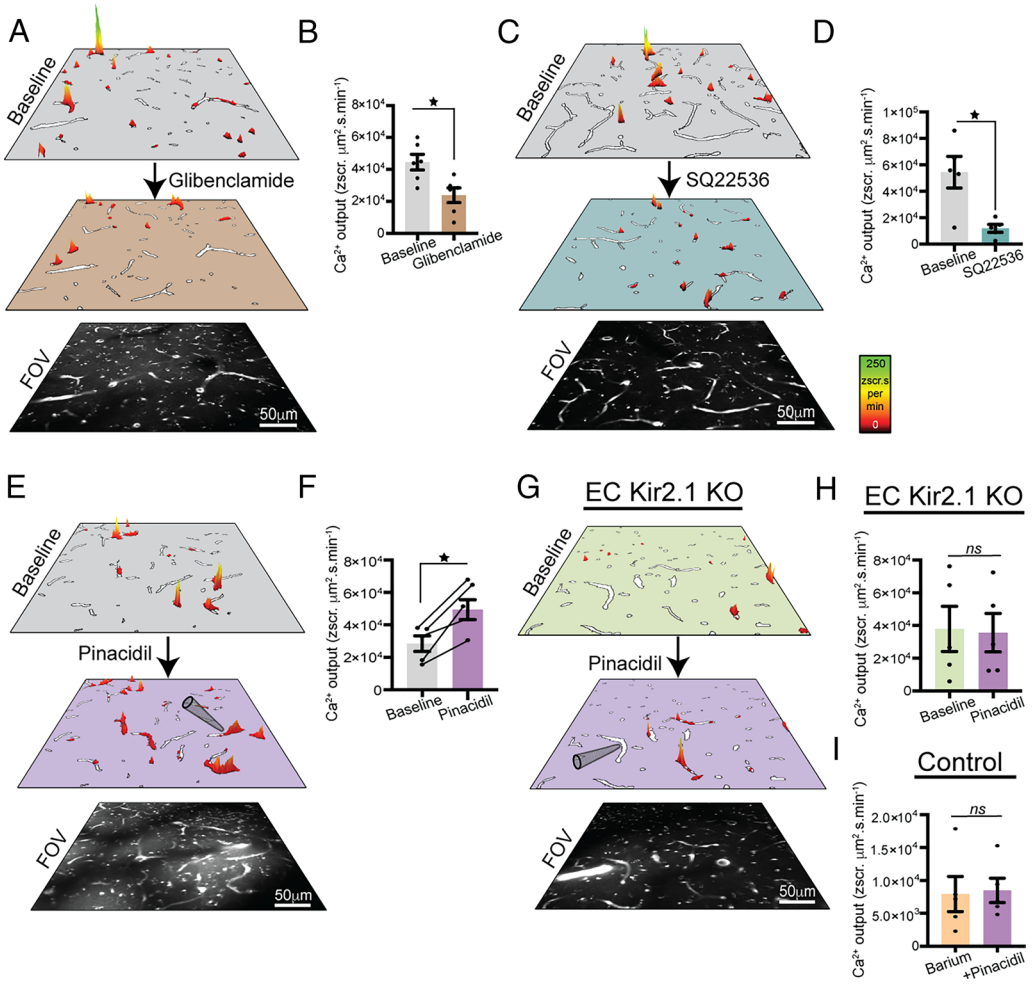

Fig. 3. K_{ATP} channel signaling intersects with Kir2.1 channels to drive long-distance Ca^{2+} signaling. (*A* and *B*) Prevalence maps (*A*) and summary data (*B*) showing cEC Ca^{2+} responses before and 20 min after surface application of the K_{ATP} inhibitor glibenclamide (10 μM) (n = 6 experiments, 6 mice; *$P < 0.05$, paired *t* test). (*C* and *D*) Prevalence maps (*C*) and summary data (*D*) showing cEC Ca^{2+} responses before and after surface application of the adenylate cyclase inhibitor SQ22536 (300 μM) (n = 5 experiments, 5 mice; *$P < 0.05$, paired *t* test). (*E–H*) Prevalence maps (*E* and *G*) and summary data (*F* and *H*) showing cEC Ca^{2+} events before and after picospritzing the K_{ATP} activator pinacidil (10 μM) (n = 5 experiments, 5 mice) in control mice (*E* and *F*) and EC Kir2.1-KO mice (*G* and *H*). (*I*) Summary data showing cEC Ca^{2+} responses to pinacidil (10 μM) in wild-type mice in the presence of barium (100 μM) (n = 5 experiments, 5 mice, *$P < 0.05$, paired *t* test; ns, not significant).

Unlike Kir2.1 channels, K_{ATP} channels are not activated by hyperpolarization and thus lack the intrinsic capacity to amplify propagating current. This led us to speculate that the ability of K_{ATP} activation to drive long-distance Ca^{2+} signals reflects its hyperpolarization-induced activation of cEC Kir2.1 channels and engagement of E-Ca coupling. To test this, we focally activated K_{ATP} channels under conditions in which Kir2.1 channels were genetically eliminated (EC-Kir2.1-KO mice) or blocked (100 μM Ba^{2+}) and measured cEC Ca^{2+} responses throughout the FOV. In both EC-Kir2.1-KO mice and in the presence of Ba^{2+}, picospritzed pinacidil (10 μM) failed to significantly increase cEC Ca^{2+} signals (Fig. 3 *G–I*), indicating that K_{ATP} channel-mediated induction of distant Ca^{2+} signaling is dependent on Kir2.1 channels.

G_qPCR-IP_3/IP_3R Signaling and Ca^{2+} Influx through TRPV4 Channels Serves a Priming Function That Supports E-Ca Coupling. Multiple neural activity-derived compounds are agonists of G_qPCR pathways in cECs. As a testament to the significance of this ongoing production and release of G_qPCR ligands, we previously found that brain-wide inhibition of baseline G_qPCR signaling with the $G\alpha_{q/11}$ inhibitory depsipeptide, FR900359, virtually eliminated (~90% reduction) cEC Ca^{2+} signals in vivo (5). Because this chemical inhibitor might also inhibit $G\alpha_{q/11}$ receptors expressed in other cell types involved in NVC, including neurons, astrocytes, and SMCs (22–25), we sought to confirm that the cEC Ca^{2+} signals observed under baseline conditions were specifically attributable to G_qPCR signaling in cECs. To this end, we used tamoxifen-inducible, brain EC-specific $G\alpha_{q/11}$-KO mice (hereafter, EC $G\alpha_{q/11}$-KO mice), in which Cre expression is driven by the *Slco1c1* promoter, which is selectively active in CNS ECs (26). To confirm the functional deletion of $G\alpha_{q/11}$ genes in ECs in our experimental context, we measured changes in somatosensory cortex CBF in response to surface application of the G_qPCR agonist, carbachol (10 μM), using laser-Doppler flowmetry. As expected, carbachol led to a robust increase in CBF in control mice, but not in EC $G\alpha_{q/11}$-KO mice (*SI Appendix*, Fig. S2 *A* and *B*). Consistent with results obtained using the pharmacological inhibitor, FR900359, we found that cEC Ca^{2+} signaling under basal conditions was strongly suppressed (~70%) in EC $G\alpha_{q/11}$-KO mice (Fig. 4 *A* and *B* and Movie S7), confirming a crucial role for $G\alpha_{q/11}$ signaling in cECs in the generation of cEC Ca^{2+} signals.

To definitively establish an obligate role for G_qPCR-IP_3/IP_3R signaling in the coupling of hyperpolarization to Ca^{2+} signaling, we measured Ca^{2+} events in vivo after providing a focal hyperpolarizing stimulus by picospritzing 10 mM K^+ (to activate Kir2.1 channels) or pinacidil (to activate K_{ATP} channels) onto ACT zone capillary segments in EC $G\alpha_{q/11}$-KO mice. Whereas both of these stimuli produced robust increases in Ca^{2+} signaling in wild-type mice (Figs. 1*F* and 3*E*), neither significantly increased cEC Ca^{2+}

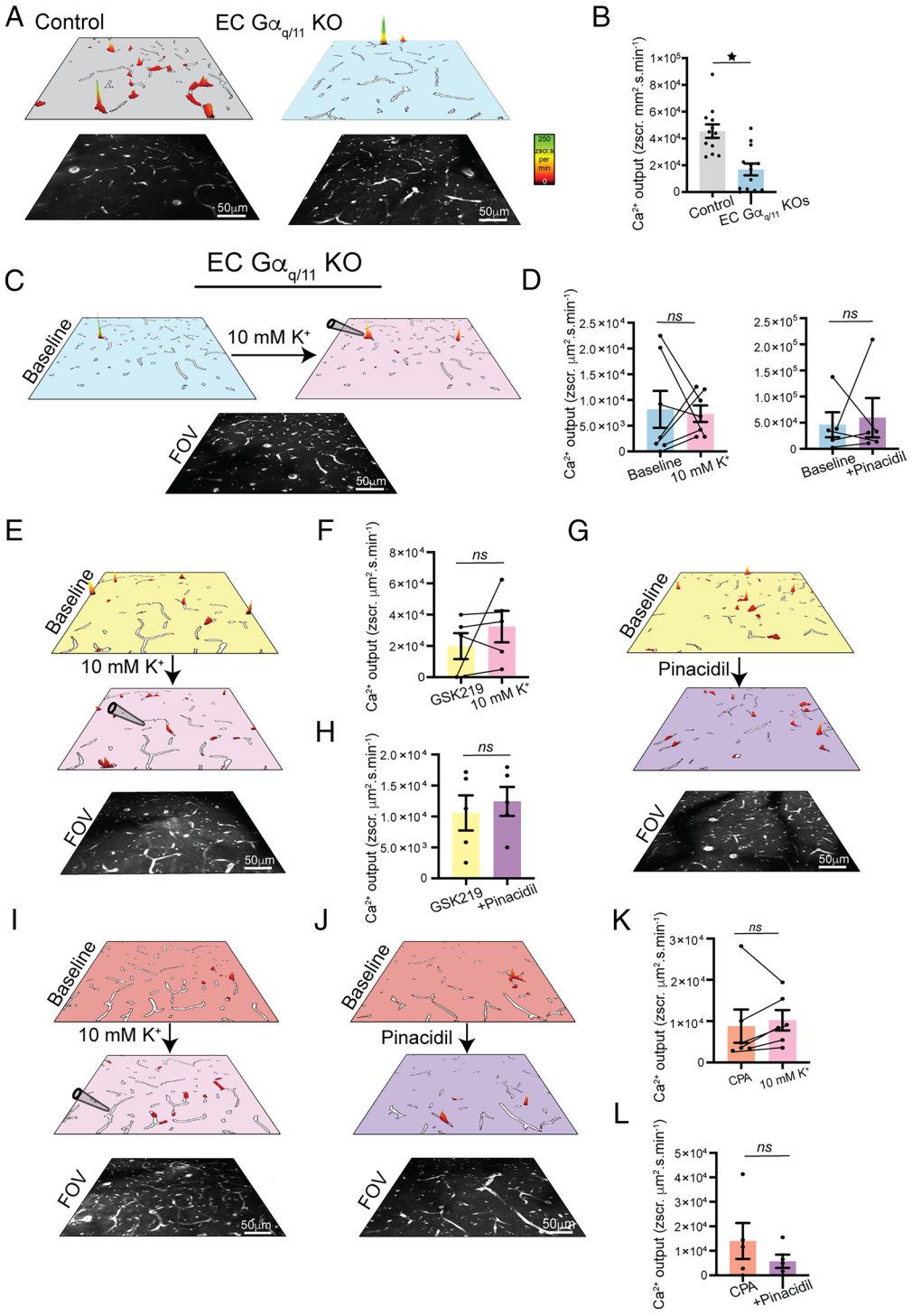

Fig. 4. Long-distance Ca^{2+} signaling mediated by E-Ca coupling is supported by a G_qPCR/IP_3/TRPV4 CICR-signaling module. (*A* and *B*) Prevalence maps (*A*) and summary data (*B*) comparing cEC Ca^{2+} events in control and EC $G_{q/11}$-KO mice (n = 11 experiments, 11 mice; *$P < 0.05$, unpaired *t* test). (*C* and *D*) Prevalence maps (*C*) and summary data (*D*, *Left*) showing cEC Ca^{2+} signals in EC $G_{q/11}$-KO mice before and after picospritzing 10 mM K^+ (n = 5 to 6 experiments, 5 to 6 mice); ns, not significant (Wilcoxon paired test). (*D*, *Right*) Summary data showing cEC Ca^{2+} signals in EC $G_{q/11}$-KO mice before and after cortical application of 10 μM pinacidil (prevalence maps not shown; n = 5 to 6 experiments, 5 to 6 mice); ns, not significant (Wilcoxon paired test). (*E–H*) Prevalence maps showing cEC Ca^{2+} signals in control mice in the presence of GSK219 (1 μM) following Picospritzing of 10 mM K^+ (*E*) or cortical application of 10 μM pinacidil (*F*) and corresponding summary data (*G* and *H*) (n = 5 experiments, 5 mice); ns, not significant (paired *t* test). (*I–L*) same as *E–H* except the control mice is injected with 0.7 mg/kg CPA (n = 5 to 6 experiments, 5 to 6 mice); ns, not significant (Wilcoxon paired test).

signals in EC $G\alpha_{q/11}$-KO mice (Fig. 4 *C* and *D*). Direct measurements of cEC membrane potential in pressurized retina preparations from EC $G\alpha_{q/11}$-KO mice revealed robust hyperpolarization from baseline following bath application of 10 mM K^+ (−45 ± 4 to −69 ± 2 mV) or pinacidil (−45 ± 4 to −86 ± 2 mV), indicating that the failure of K^+ and pinacidil to generate Ca^{2+} signals in EC $G\alpha_{q/11}$-KO mice does not reflect an inability of these agents to effectively hyperpolarize the membrane potential of cECs in these mice (*SI Appendix*, Fig. S3). Collectively, these findings suggest that on-going G_qPCR signaling in cECs acts as a "priming" step, creating the intracellular preconditions necessary for coupling electrical and Ca^{2+} signaling. They also indicate that hyperpolarization

alone—that is, without significant G_qPCR activity, and by extension, IP_3 production (see below)—is insufficient to drive E-Ca coupling.

In our previous studies, we reported that TRPV4 channels are part of an IP_3R-dependent CICR mechanism involved in regulating baseline cEC Ca^{2+} signals (5). Here, we directly tested the involvement of this TRPV4/IP_3R/IP_3R-dependent CICR mechanism in mediating the Ca^{2+}-signaling component of E-Ca coupling by measuring Ca^{2+} responses in cECs remote from a focal hyperpolarizing stimulus. To this end, we picospritzed 10 mM K^+ onto ACT zone capillaries of wild-type *Cdh5*-GCaMP8 mice, with and without surface application of the selective TRPV4 channel inhibitor, GSK2193874 (hereafter, GSK219; 1 μM), and recorded Ca^{2+} signals. In the absence of GSK219, 10 mM K^+ and pinacidil induced a significant increase in cEC Ca^{2+} signaling throughout the FOV; this effect was abolished in the presence of GSK219 (Fig. 4 *E–H*). Collectively, these observations confirm the essential role of TRPV4 channels in mediating the coupling of hyperpolarization with Ca^{2+} signaling. They also indicate that capillary Ca^{2+} events are dependent on G_qPCR-IP_3/IP_3R-TRPV4 channel signaling and reflect the operation of an IP_3R-dependent CICR mechanism.

Intracellular Ca^{2+} Store Recharging Is Required for Basal Ca^{2+} Activity and E-Ca Coupling. In our previous report (5), we showed that maneuvers that disrupt intracellular Ca^{2+} signaling, such as depleting ER Ca^{2+} stores by inhibiting SERCA-mediated store refilling with cyclopiazonic acid (CPA), blocking IP_3Rs with xestospongin C or 2-aminoethoxydiphenyl borate, or inhibiting CICR by chelating intracellular Ca^{2+} with EGTA-AM, inhibited ongoing (baseline) Ca^{2+} signals to varying degrees (~55 to 80%), with CPA producing the greatest inhibition (~80%). To determine whether ER Ca^{2+} store release/refilling is similarly central to the E-Ca coupling-dependent Ca^{2+} signaling following a focal hyperpolarizing stimulus, we intravenously injected CPA (0.7 mg/kg) or vehicle into *Cdh5*-GCaMP8 mice and then measured Ca^{2+} signals throughout the FOV in the barrel cortex after 10 mM K^+ or pinacidil exposure. Consistent with results obtained for baseline Ca^{2+} signaling, Ca^{2+} signals evoked in response to a hyperpolarizing stimulus were abrogated under conditions in which SERCA activity was inhibited (Fig. 4 *I–L*), highlighting the importance of intracellular Ca^{2+} store dynamics in the operation of the E-Ca coupling mechanism.

Computation Modeling Supports a Central Role for Kir2.1 Channels, Ca^{2+} Influx, and Store Recharging in E-Ca Coupling. E-Ca coupling can be conceptualized as a rapidly traveling electrical (hyperpolarizing) wave that leaves a trail of "embers"—Ca^{2+} signals—in its wake. This conceptualization invites the application of a genetically engineered voltage-indicator (GEVI) mouse model to directly monitor changes in membrane potential throughout the vasculature in relation to observed Ca^{2+} signals. However, no suitable GEVI mouse model capable of detecting hyperpolarization in ECs is currently available. Thus, we turned to computational modeling to predict the relationship between Kir2.1 and K_{ATP} stimulation and cEC Ca^{2+} signaling in a simulated microvascular network.

We have previously used an in silico approach to examine how local hyperpolarizing stimuli in the capillary endothelium propagate throughout a reconstructed microvascular network in a cortical volume of 0.5 μL (27). The resulting model comprises 10^4 cells and simulates membrane potential (V_m) and Ca^{2+} dynamics in cEC, each of which is electrically coupled though gap junctions (Fig. 5*A*) or saturating pinacidil, allowing currents to propagate along the network. Here, we applied this detailed multicellular model of the cerebral microcirculation to investigate mechanisms that underlie the observed Ca^{2+} activity and to explore the biophysical determinants of E-Ca coupling in capillary networks. Representative simulations (Fig. 5 *B* and *C*) performed using a modification of this "virtual voltage-sensor mouse" [see *Materials and Methods* and (27) for details] predicted stimulatory requirements for physiologically relevant capillary network hyperpolarization. Specifically, an

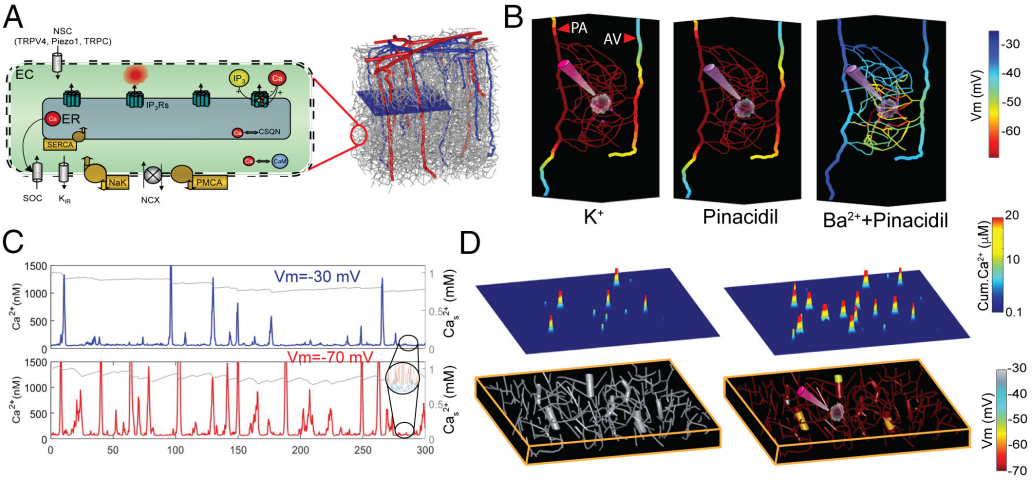

Fig. 5. Mathematical modeling of E-Ca coupling. (*A*) Multicellular model examining electrical and Ca^{2+} dynamics and their propagation in a reconstructed cerebral microvascular network. Electrical and Ca^{2+} responses are simulated in 10^4 cECs within 0.5 μL of cortex. Each cEC model is based on previous models (27) and accounts for important membrane components (e.g., Kir, K_{ATP}, NSC channels, PMCA pumps). Cytosolic subdomains contain an ER store and a cluster of IP_3Rs (n = 20). Basal IP_3 concentration in each cEC is randomly selected from an exponential distribution. (*B*) Simulated focal application of K^+ (10 mM) or a maximally activating concentration of pinacidil on 7 cECs produced a robust hyperpolarization (red; see mV scale bar) of the local vascular network and part of the PA and AV under control conditions but not after blockade of Kir activity (Ba^{2+} + Pinacidil). (*C*) Stochastic Ca^{2+} events in a cytosolic subdomain with an IP_3 cluster. Site is assumed to have basal IP_3 levels ($[IP_3] = 2 \times EC_{50,\,m}$). Membrane hyperpolarization increases the Ca^{2+} electrochemical gradient and transmembrane Ca^{2+} influx through NSC channels. The higher frequency of Ca^{2+} events is attributable to higher basal cytosolic Ca^{2+} levels (insert) and more rapid recharging of the store after each event (gray line, *Right* axis). (*D*) Membrane potential (*Bottom* row) and cumulative Ca^{2+} activity over 1 min of simulation (*Top* row) in a 425 × 425 × 50 μm^3 tissue volume. Stochastic opening of IP_3Rs leads to spontaneous Ca^{2+} events in "active" sites with high IP_3 levels (*Left*). Focal K^+ stimulation (10 mM on 7 cECs) (*Right*) resulted in robust hyperpolarization of the vascular network and an increase in Ca^{2+} activity from 17 events/min (*Left*) to 48 events/min (*Right*).

examination of hyperpolarizing activity in a small capillary network segment between a feeding arteriole and a draining venule (Fig. 5*B*) showed that, under experimental-mimetic conditions (10 mM K^+ or saturating pinacidil onto 5 to 7 cECs) and using physiologically realistic values for important parameters (i.e., Kir2.1, K_{ATP} conductances, and gap junctional resistance; see *Materials and Methods*), focal stimulation was capable of initiating a hyperpolarizing current in the stimulated cells that propagates throughout the capillary network and segments of the penetrating arteriole (PA) and ascending venule (AV).

Computational modeling further corroborated experimental findings that local K_{ATP} channel-mediated hyperpolarization spreads through the capillary network through subsequent activation of cEC Kir2.1 channels. These simulations showed that focal activation of K_{ATP} channels with pinacidil (5 to 7 cECs) produces robust, Kir2.1-dependent local and propagating hyperpolarization (Fig. 5*B*), reaffirming the role of cEC Kir activity as a critical determinant of the ability of the capillary network to propagate hyperpolarizing stimuli. These simulations support a role for the cEC Kir2.1 channel as a mediator of the conducted electrical signal in addition to its role as a K^+ sensor, and demonstrate how experimentally induced focal stimulation can robustly hyperpolarize the capillary network within the FOV to drive Ca^{2+} activity.

The cEC model (27) was extended to account for stochastic IP_3R dynamics and predict spontaneous Ca^{2+} activity in cECs (*Materials and Methods*) (Fig. 5*A* and *SI Appendix*, Fig. S4*A*). Fig. 5 *C*, *Top* depicts a representative simulation of stochastic Ca^{2+} events from an IP_3R cluster within a cEC. Basal IP_3 levels (reflecting G_qPCR activity) drive stochastic openings of IP_3Rs in the cluster as well as fluctuations in resting cytosolic Ca^{2+} levels, which can be robustly amplified through a CICR mechanism when they cross a threshold value. The resulting pronounced increases in intracellular Ca^{2+} concentration—Ca^{2+} events—are terminated by the Ca^{2+}-dependent inactivation of IP_3Rs (*SI Appendix*, Fig. S4*A*). Membrane hyperpolarization (Fig. 5 *C*, *Bottom*) increases the Ca^{2+} electrochemical gradient and transmembrane Ca^{2+} influx through open NSC channels. The predicted Ca^{2+} influx is physiologically relevant: It can increase basal cytosolic Ca^{2+} levels (Fig. 5 *C*, *Inset*) and allows for faster recharging of stores following their depletion during a Ca^{2+} event (Fig. 5*C*, gray line). The increases in cytosolic Ca^{2+} levels and recharging of Ca^{2+} stores supported by the model increase IP_3R open probability and Ca^{2+} efflux through open IP_3Rs, respectively (Fig. 5*C*). Taken together, these two effects increase the probability that an IP_3R cluster "fires" and modulates the frequency of Ca^{2+} events in an "active" cEC site. Simulations were performed assuming cECs with varying basal IP_3 concentrations in a simulated FOV representing a slice of brain tissue, 425 × 425 × 50 μm^3 volume, containing ~180 cECs (Fig. 5*C*). The model demonstrates that stochastic opening of IP_3Rs within a cluster in conjunction with CICR results in robust Ca^{2+} events in a subset of "active" cECs with sufficient basal IP_3 levels (Fig. 5*D* and *SI Appendix*, Fig. S4*B*). Following a hyperpolarizing stimulus (10 mM K^+ onto 5 to 7 cECs), the number of Ca^{2+} events increased by ~280%, from ~17 events/min to 48 events/min (Fig. 5*D*). Notably, the simulated increase in Ca^{2+} activity with membrane hyperpolarization is in agreement with experiments in which we inhibited or initiated electrical signaling, supporting the conclusion that the E-Ca mechanism can robustly modulate Ca^{2+} activity (Fig. 1 *E* and *G*). The model also shows that hyperpolarization-induced transmembrane Ca^{2+} influx translates to more frequent Ca^{2+} events in active sites, but also the recruitment of sites with lower basal IP_3 levels in the simulated FOV (Fig. 5*D* and *SI Appendix*, Fig. S4*C*). The overall increase in the prevalence of Ca^{2+} events within the capillary network can be visualized as a conducted hyperpolarizing wave igniting Ca^{2+} signals in its wake (Movie S8). The model highlights the central role of IP_3 signaling and transmembrane Ca^{2+} influx in modulating Ca^{2+} activity and reinforces experimental results on the role of store recharging. It also provides mechanistic explanations for salient features of this activity at cellular and network levels.

Discussion

Here, we demonstrate that long-range electrical signaling increases the driving force for Ca^{2+} entry into cECs through plasma membrane Ca^{2+}-permeable cation channels. This process, which we have termed E-Ca coupling, depends on the biophysical properties of the Kir2.1 channel—particularly its steep activation by hyperpolarization—which enables it to amplify an electrical (hyperpolarizing) signal as it travels from cell to cell along the "wire-like" network of capillaries. It also depends on 1) TRPV4 channels (and possibly other NSC channels), which provide a conduit through which Ca^{2+} can flow into the cell down its electrochemical gradient; and 2) G_qPCR signaling, which provides the IP_3 necessary to sensitize IP_3Rs to activation by intracellular Ca^{2+} and subsequently release Ca^{2+} from the ER via a CICR mechanism. Thus, as spreading waves of Kir2.1-mediated hyperpolarization pass through cECs, they increase Ca^{2+} influx via TRPV4 channels in cECs at a distance from the site of stimulation, evoking optically detectable Ca^{2+} signals—provided these cECs are sufficiently primed by G_qPCR activity. Importantly, we further established that G_sPCR-K_{ATP} channel signaling feeds into this mechanism at the level of the Kir2.1 channel such that hyperpolarization induced by activation of K_{ATP} channels activates Kir2.1 channels, which provide a "booster" function that enables what would otherwise be a localized hyperpolarization to propagate from cell to cell over longer distances.

Kir2.1 Channel-Mediated Hyperpolarization Is the Linchpin for the E-Ca Coupling Process. The Kir2.1 channel is uniquely suited to detecting neuronal activity and translating it into a vascular response. No other channel shares its combination of dual activation by extracellular K^+ and hyperpolarization (17). The specific sensitivity of Kir2.1 channels to activation by extracellular K^+ enables these channels to respond to K^+ released into the extracellular space by neurons during an action potential. Because Kir2.1 channels are activated by hyperpolarization and are expressed in all cECs, the hyperpolarization produced by their activation in one cell has the potential to activate these channels in an adjacent cell, setting the stage for cell-to-cell regenerative propagation of the original hyperpolarization signal (1, 27). One important implication of this property is that hyperpolarization produced by any mechanism can activate Kir2.1 channels and "piggyback" on the regenerative potential of these channels, enabling otherwise local signals to propagate.

E-Ca Coupling Provides a Mechanism for Pseudopropagation of Ca^{2+} Signals. Although cell-to-cell propagation of Ca^{2+} signals within the vasculature has been reported to occur in certain contexts (28–31), no general mechanism for long-distance transfer of Ca^{2+} signals between vascular cells has been convincingly demonstrated. Evidence has been presented for an extracellular mediator/membrane receptor mechanism (e.g., ATP/Panx1) (29) which is enabled by Kir2.1 channels (32). Our recent work mirrors this theme, showing that neuronal activity-dependent Ca^{2+} signals

in brain cECs, monitored in vivo, do not travel from cell to cell but instead are confined to the cell in which they are initiated (5). What does travel from cell to cell is membrane hyperpolarization. And as it does, it superimposes an additional electrical driving force upon the inherent electrochemical gradient for Ca^{2+} in cECs, as described by the GHK relationship. The resulting augmented electrochemical gradient intensifies the driving force for Ca^{2+} entry, increasing Ca^{2+} influx into cECs along the path of the propagating hyperpolarization. In a very real sense, an initial hyperpolarizing signal is converted to Ca^{2+} signals that manifest stochastically at sites along the stimulated microvasculature that can be far removed from the original stimulus.

G_qPCR Signaling Primes cECs to Respond to Propagating Hyperpolarization. G_qPCR signaling serves a key priming function by establishing the necessary preconditions that enable an increase in the driving force for Ca^{2+} entry to produce an optically detectable Ca^{2+} signal. The centrality of G_qPCR signaling in this E-Ca coupling response is predicted by model results and corroborated by the finding that long-distance Ca^{2+} signaling was largely absent in EC $G\alpha_{q/11}$-KO mice and virtually eliminated by the selective $G\alpha_{q/11}$ inhibitor, FR900359.

The increase in intracellular IP_3 levels arising from G_qPCR-dependent, PLC-mediated hydrolysis of PIP_2 sensitizes IP_3Rs to intracellular Ca^{2+}, providing the molecular impetus for the release of Ca^{2+} from ER stores. Upon binding IP_3, the IP_3R undergoes a conformational change that increases its affinity for Ca^{2+}, which binds to a site in a cytoplasm-facing region of the IP_3R. Importantly, Ca^{2+} has dual effects on the IP_3R: At lower concentrations, it serves a CICR function, acting as an agonist to promote release of Ca^{2+} from the ER; at higher concentrations, it acts as an antagonist to inhibit or prevent further release of Ca^{2+} from ER stores (33–35). These dynamics likely enable the initiation and termination of Ca^{2+} mobilization during an event. Model simulations incorporating clusters of IP_3Rs in "G_qPCR-primed" cECs can reproduce the stochastic Ca^{2+} events observed experimentally. Furthermore, model and experimental results demonstrate that hyperpolarization-induced increases in Ca^{2+} influx can increase this Ca^{2+} activity. Intercellular variations in cytosolic/store Ca^{2+} concentration, G_qPCR activity—and thus IP_3—or transmembrane Ca^{2+} permeability can be expected to contribute stochasticity to E-Ca coupling responses. This likely accounts for the observation that Ca^{2+} signals are only detected in a subset of cECs.

Our results suggest that Ca^{2+} influx—the crucial counterpart to sensitized IP_3Rs necessary to complete the CICR machinery—is primarily mediated by the TRPV4 channel. Although the increased electrical driving force produced by membrane hyperpolarization can promote Ca^{2+} entry through any Ca^{2+}-permeable ion channel, the number and open probability of these channels need to be appropriate to support sufficient Ca^{2+} entry. In the case of the TRPV4 channel, an important mechanism for increasing open probability is through depletion of PIP_2 by G_qPCR signaling, which disinhibits this channel (7). cECs express multiple types of NSC channels, including TRPV4, TRPA1, Piezo1, and STIM/ORAI1/ORAI3 (5, 29, 36, 37). Among these cation channels, those that are constitutively active can support Ca^{2+} activity through E-Ca coupling, whereas those activated by store or G_qPCR-mediated PIP_2 depletion (ORAI1/ORAI3, TRPV4, TRPA1, TRPC3) may support increase in Ca^{2+} activity independent of electrical signaling.

K_{ATP} Channel Signaling Intersects with the Kir2.1 Channel-Dependent E-Ca Coupling Mechanism. Our findings also provide a demonstration that K_{ATP} channel-mediated hyperpolarization intersects with Kir2.1-mediated signaling in cECs to drive CICR-dependent increases in long-range Ca^{2+} signaling. Under physiological conditions, this mechanism would be engaged by neuronally derived agonists, such as adenosine and neuropeptides (e.g., CGRP), which activate G_sPCRs, leading to stimulation of AC, increased cAMP levels/PKA activity, and PKA-mediated activation of K_{ATP} channels. Collectively, these observations establish a direct link between G_sPCR signaling and the G_qPCR/IP_3/TRPV4 functional module. Interestingly, our data on Ca^{2+} signal induction, hyperpolarization of cECs (retina preparation), and modeling results are in alignment with the idea that focal activation of K_{ATP} channels in the context of patent Kir2.1 signaling amplifies Kir2.1 channel-mediated hyperpolarization, and thus E-Ca coupling, as reflected in a greater increase in Ca^{2+} signals (50% vs. 35%) and hyperpolarization (−50 mV vs. −28 mV) compared with focal activation of Kir2.1 channels alone. Future studies investigating vascular EC Ca^{2+} signals in mice expressing GEVIs (when they become available), should shed additional light on these relationships.

Focally Induced Hyperpolarization Spreads in All Directions. It has been shown that vascular signals generated by physiological stimuli at the capillary level in the deep parenchyma are capable of retrograde propagation and dilation of upstream arterioles and pial vessels (38–41), findings consistent with our demonstration that focal stimulation (picospritzed K^+) of capillaries in vivo dilates feeding arterioles via Kir2.1-mediated membrane hyperpolarization (1). The prevailing assumption in the field is that such directional signaling is a hallmark of NVC, and that without it, NVC as we know it would not be possible. Against this backdrop, we found that hyperpolarizing signals generated in vivo by focal stimulation of cECs with K^+ or pinacidil propagate in all directions from the stimulus site with no bias toward arterioles or venules. While this makes perfect sense given the molecular and electrochemical mechanisms involved and the conceptualization of the cerebral capillary network as a system of wires, it raises the question of how directionality arises in the intact animal. It is possible that excitatory-interneuron circuits, which are bypassed by our focal cEC-stimulation paradigm, impart directionality to the otherwise omnidirectional electrical signal or shape its impact on the vasculature. In addition, contractile pericytes, which are likely electrically coupled to cECs and are strategically positioned upstream of signals arising deeper in the capillary bed, could contribute to directionality by selectively dilating along the retrograde path in response to the passing electrical current.

Interestingly, a branch point/distance analysis following focal stimulation provided insights into the structure of the capillary network, revealing a linear distance between a PA and an AV of ~400 μm, closely corresponding to a single vibrissae cortical volume (~500 μm) (42). This analysis also showed an average of 8 to 10 capillary branches—which is equal to the number of cECs—between an arteriole and a venule, an estimate consistent with a previous seminal analysis of the rodent brain microvasculature by Kleinfeld's group (20).

Kir2.1-Mediated Hyperpolarization Propagation Mode. Our previous modeling work predicts four possible electrical propagation modes in capillary networks: 1) passive/electrotonic, 2) Kir-facilitated conduction (rapidly developing, like an electric spark), 3) slower and near-simultaneous transitions of a population of cells to an excitable hyperpolarized state (like a slow rising tide), and 4) regenerative signaling transmitted over long distances (like a propagating wave) (27). This last mechanism is akin to the propagation of an action potential. The type of spreading behavior

predicted depends primarily on Kir2.1 current density (G_{Kir}), the number of cECs activated, and gap junctional resistance (R_{gj}). In a previous study, we modeled hyperpolarization of upstream arterioles based on experiments employing an ex vivo capillary-PA (CaPA) preparation (27) in which 10 mM K^+ is picospritzed onto the extremities of capillaries attached to an upstream, pressurized arteriole segment—an experimental paradigm that closely parallels the in vivo experimental approach used here. Using G_{Kir} values estimated from these simulations, and holding other parameter values constant, the model predicts regenerative propagation. In contrast, values of G_{Kir} estimated from single-cell electrophysiology experiments generally fall in a range that would fail to support this propagation mode. Thus, at this point, it is not entirely clear which propagation mode Kir2.1 promotes and under what conditions. However, evidence suggests that the propagation of hyperpolarizing signals in capillary networks does not simply reflect passive spread (27). Consistent with limited passive spread of charge, Picospritzing a depolarizing concentration of K^+ (60 mM) onto capillaries in a CaPA preparation does not constrict the upstream arteriole (1).

The ability of Kir2.1 channels to mediate significant amplification of a propagating signal reflects their steep activation by hyperpolarization. Because K_{ATP} channels are not activated by hyperpolarization, activation of these channels should not lead to regenerative hyperpolarization on its own; thus, K_{ATP} channel-induced hyperpolarizing signals are limited to passive spread in the absence of Kir2.1 channels. Indeed, we did not detect an increase in Ca^{2+} activity by K_{ATP} activation in the absence of cEC Kir2.1 channels.

Unanswered Questions and Future Directions. A prominent unanswered—or incompletely answered—question is how G_qPCR activity-dependent PIP_2 depletion, which is known to have reciprocal effects on Kir2.1 channels (inhibition) and TRPV4 channels (disinhibition), fits into the E-Ca coupling framework. Our findings in this regard are somewhat paradoxical. Whereas PIP_2 depletion seems to be intimately involved in enhancing TRPV4 activity and thereby facilitating Ca^{2+} influx, CICR, and store refilling, the predicted inhibition of Kir2 activity was not evident in our experimental paradigm. Differential kinetics of Kir2.1 inhibition and TRPV4 disinhibition is one possible explanation. Our previous single-cell electrophysiology studies showed that inhibition of Kir2.1 channel activity by PIP_2 depletion takes up to 20 min to fully manifest (6), a time frame that would place this inhibitory effect outside our experimental window (~6 min). Literature reports that this inhibition occurs within seconds in other cell types (e.g., neurons) (43, 44) and expression systems add intrigue to this question.

The role of pericytes in E-Ca coupling is not known. Our previous work (2) and earlier studies by Puro and colleagues (45, 46) suggest that pericytes and endothelial cells are electrically coupled. However, the nature of coupling and its bidirectionally are unclear. It is possible that pericytes could act as current sinks for electrical signaling in cECs, hindering electrical signaling in cECs by passing depolarizing currents into them. They could also act as amplifiers of cEC electrical signaling based on the nature and magnitude of pericyte K+ currents (47). These are active areas of investigation.

How E-Ca coupling impacts physiological processes is an area of active investigation. The increased driving force for Ca^{2+} entry into cECs that occurs as a consequence of propagating hyperpolarization from sites of neural activity in response to physiological stimuli increases the spatiotemporal prevalence of Ca^{2+}-release sites throughout the capillary network. This could aid in providing sufficient Ca^{2+} for local blood flow control (e.g., via an eNOS/NO mechanism) along the often-considerable distances from the sites of neural activity to the feeding arteriole and AV. Hemodynamic responses to single-whisker stimulation propagate beyond the principle cortical volume (42, 48–50), potentially perfusing the entire column and beyond. E-Ca coupling, which provides an elegant mechanism for coordinating Ca^{2+} events by linking hyperpolarization and enhanced Ca^{2+} signaling, could ensure the effective and directed routing of blood through the tangle of capillaries to areas in need. Taking the finding of omnidirectional electrical signaling at face value, the downstream spread of this signal could also contribute to increasing venous EC permeability, possibly aiding in the clearance of metabolic waste or supporting immune cell transcytosis. In addition to these roles, E-Ca coupling may also be involved in resolving capillary stalls. In summary, our study recasts capillary endothelial cells as excitable cells and the coupling between excitation (hyperpolarization) and Ca^{2+} bridges the gap between fast, long-range electrical signaling and slower, local Ca^{2+} events that supply and direct blood flow to areas of need.

Materials and Methods

All animals were used in accordance with protocols approved by the Institutional Animal Care and Use Committee of the University of Vermont. Detailed descriptions of procedures and materials required for craniotomy, in vivo imaging, membrane potential measurements, image analysis, and mathematical modeling/simulations are included in *SI Appendix, Methods*.

Statistics. Statistical testing was performed using GraphPad Prism 10 software. Data are expressed as means ± SEM, and a P-value ≤ 0.05 was considered significant. All experiments were paired, unless otherwise stated. Data were tested for normality using a Shapiro–Wilk test prior to application of the appropriate parametric or nonparametric statistical test. Stars denote significant differences; "ns" indicates nonsignificant comparisons. Statistical tests are noted in figure legends. All *t* tests were two-sided. Sample sizes were estimated based on similar experiments performed previously in our laboratory. Data collection was not performed blinded to the conditions of the experiments. Littermates were randomly assigned to experimental groups; no further randomization was performed.

Data, Materials, and Software Availability. All study data and custom code are included in the article and/or supporting information.

ACKNOWLEDGMENTS. We thank D. Enders, N. Cashen, and T. Wellman for technical assistance; T. A. Longden (University of Maryland) for help with some experimental data acquisition; and J. Wenzel (University of Lübeck), M. Schwaninger (University of Lübeck), and Stefan Offermanns (Max Planck Institute) for providing brain endothelial specific $G\alpha_{q/11}$-knockout mice. Research reported in this publication was supported by the National Institute of Aging and National Institute of Neurological Disorders and Stroke (K99-AG-075175 to A.M.; R01-NS-110656, RF1-NS-128963-01 to M.T.N.; and R01-NS-119971 to N.M.T.), the National Institute of General Medical Sciences (P20-GM-135007 to M.T.N.), the National Heart, Lung, and Blood Institute (R35-HL-140027 to M.T.N.), American Heart Association Career Development Award (856791 to A.M.) and postdoctoral fellowship (20POST35210155 to A.M.), the Totman Medical Research Trust (to M.T.N.), the European Union Horizon 2020 Research and Innovation Programme (Grant Agreement 666881, SVDs@target to M.T.N.); and Leducq Foundation Transatlantic Network of Excellence (International Network of Excellence on Brain Endothelium: A Nexus for Cerebral Small Vessel Disease, MTN).

Author affiliations: [a]Department of Pharmacology, University of Vermont, Burlington, VT 05405; [b]Department of Biomedical Engineering, Florida International University, Miami, FL 33174; and [c]Division of Cardiovascular Sciences, University of Manchester, Manchester M13 9PL, United Kingdom

Author contributions: A.M., N.M.T., D.H.-E., and M.T.N. designed research; A.M., T.H., and N.M.T. performed research; A.M., G.W.H., T.H., and N.M.T. analyzed data; and A.M., G.W.H., N.M.T., D.H.-E., and M.T.N. wrote the paper.

Reviewers: J.A.F., Augusta University; and M.F.N., University of California, Davis.

The authors declare no competing interest.

1. T. A. Longden *et al.*, Capillary K(+)-sensing initiates retrograde hyperpolarization to increase local cerebral blood flow. *Nat. Neurosci.* **20**, 717–726 (2017).
2. A. L. Gonzales *et al.*, Contractile pericytes determine the direction of blood flow at capillary junctions. *Proc. Natl. Acad. Sci. U.S.A.* **117**, 27022–27033 (2020).
3. A. Mughal, M. T. Nelson, D. Hill-Eubanks, The post-arteriole transitional zone: A specialized capillary region that regulates blood flow within the CNS microvasculature. *J. Physiol.* **601**, 889–901 (2023).
4. D. A. Hartmann, V. Coelho-Santos, A. Y. Shih, Pericyte control of blood flow across microvascular zones in the central nervous system. *Annu. Rev. Physiol.* **84**, 331–354 (2022).
5. T. A. Longden *et al.*, Local IP(3) receptor-mediated Ca(2+) signals compound to direct blood flow in brain capillaries. *Sci. Adv.* **7**, eabh0101 (2021).
6. O. F. Harraz, T. A. Longden, F. Dabertrand, D. Hill-Eubanks, M. T. Nelson, Endothelial GqPCR activity controls capillary electrical signaling and brain blood flow through PIP(2) depletion. *Proc. Natl. Acad. Sci. U.S.A.* **115**, E3569–E3577 (2018).
7. O. F. Harraz, T. A. Longden, D. Hill-Eubanks, M. T. Nelson, PIP(2) depletion promotes TRPV4 channel activity in mouse brain capillary endothelial cells. *Elife* **7**, e38689 (2018).
8. M. Sancho *et al.*, Adenosine signaling activates ATP-sensitive K(+) channels in endothelial cells and pericytes in CNS capillaries. *Sci. Signal.* **15**, eabl5405 (2022).
9. J. M. Quayle, M. T. Nelson, N. B. Standen, ATP-sensitive and inwardly rectifying potassium channels in smooth muscle. *Physiol. Rev.* **77**, 1165–1232 (1997).
10. Q. Li, D. G. Puro, Adenosine activates ATP-sensitive K(+) currents in pericytes of rat retinal microvessels: Role of A1 and A2a receptors. *Brain Res.* **907**, 93–99 (2001).
11. T. Kleppisch, M. T. Nelson, ATP-sensitive K+ currents in cerebral arterial smooth muscle: Pharmacological and hormonal modulation. *Am. J. Physiol.* **269**, H1634–H1640 (1995).
12. J. M. Quayle, A. D. Bonev, J. E. Brayden, M. T. Nelson, Calcitonin gene-related peptide activated ATP-sensitive K+ currents in rabbit arterial smooth muscle via protein kinase A. *J. Physiol.* **475**, 9–13 (1994).
13. D. A. Hartmann *et al.*, Brain capillary pericytes exert a substantial but slow influence on blood flow. *Nat. Neurosci.* **24**, 633–645 (2021).
14. N. R. Klug *et al.*, Intraluminal pressure elevates intracellular calcium and contracts CNS pericytes: Role of voltage-dependent calcium channels. *Proc. Natl. Acad. Sci. U.S.A.* **120**, e2216421120 (2023).
15. T. A. Longden, F. Dabertrand, D. C. Hill-Eubanks, S. E. Hammack, M. T. Nelson, Stress-induced glucocorticoid signaling remodels neurovascular coupling through impairment of cerebrovascular inwardly rectifying K+ channel function. *Proc. Natl. Acad. Sci. U.S.A.* **111**, 7462–7467 (2014).
16. K. Ballanyi, J. Doutheil, J. Brockhaus, Membrane potentials and microenvironment of rat dorsal vagal cells in vitro during energy depletion. *J. Physiol.* **495**, 769–784 (1996).
17. T. A. Longden, M. T. Nelson, Vascular inward rectifier K+ channels as external K+ sensors in the control of cerebral blood flow. *Microcirculation* **22**, 183–196 (2015).
18. J. M. Quayle, J. G. McCarron, J. E. Brayden, M. T. Nelson, Inward rectifier K+ currents in smooth muscle cells from rat resistance-sized cerebral arteries. *Am. J. Physiol.* **265**, C1363–C1370 (1993).
19. K. K. Bradley *et al.*, Kir2.1 encodes the inward rectifier potassium channel in rat arterial smooth muscle cells. *J. Physiol.* **515**, 639–651 (1999).
20. X. Ji *et al.*, Brain microvasculature has a common topology with local differences in geometry that match metabolic load. *Neuron* **109**, 1168–1187.e13 (2021).
21. M. T. Nelson, Y. Huang, J. E. Brayden, J. Hescheler, N. B. Standen, Arterial dilations in response to calcitonin gene-related peptide involve activation of K+ channels. *Nature* **344**, 770–773 (1990).
22. D. Billups, B. Billups, R. A. Challiss, S. R. Nahorski, Modulation of Gq-protein-coupled inositol trisphosphate and Ca2+ signaling by the membrane potential. *J. Neurosci.* **26**, 9983–9995 (2006).
23. E. Shigetomi, Y. J. Hirayama, K. Ikenaka, K. F. Tanaka, S. Koizumi, Role of purinergic receptor P2Y1 in spatiotemporal Ca(2+) dynamics in astrocytes. *J. Neurosci.* **38**, 1383–1395 (2018).
24. G. Kauffenstein, I. Laher, K. Matrougui, N. C. Guerineau, D. Henrion, Emerging role of G protein-coupled receptors in microvascular myogenic tone. *Cardiovasc. Res.* **95**, 223–232 (2012).
25. H. Kaur *et al.*, Single-cell profiling reveals heterogeneity and functional patterning of GPCR expression in the vascular system. *Nat. Commun.* **8**, 15700 (2017).
26. J. Wenzel *et al.*, Impaired endothelium-mediated cerebrovascular reactivity promotes anxiety and respiration disorders in mice. *Proc. Natl. Acad. Sci. U.S.A.* **117**, 1753–1761 (2020).
27. A. Moshkforoush *et al.*, The capillary Kir channel as sensor and amplifier of neuronal signals: Modeling insights on K(+)-mediated neurovascular communication. *Proc. Natl. Acad. Sci. U.S.A.* **117**, 16626–16637 (2020).
28. Y. N. Tallini *et al.*, Propagated endothelial Ca2+ waves and arteriolar dilation in vivo: Measurements in Cx40BAC GCaMP2 transgenic mice. *Circ. Res.* **101**, 1300–1309 (2007).
29. P. Thakore *et al.*, Brain endothelial cell TRPA1 channels initiate neurovascular coupling. *Elife* **10**, e63040 (2021).
30. T. R. Uhrenholt, T. L. Domeier, S. S. Segal, Propagation of calcium waves along endothelium of hamster feed arteries. *Am. J. Physiol. Heart Circ. Physiol.* **292**, H1634–H1640 (2007).
31. P. Bagher, M. J. Davis, S. S. Segal, Visualizing calcium responses to acetylcholine convection along endothelium of arteriolar networks in Cx40BAC-GCaMP2 transgenic mice. *Am. J. Physiol. Heart Circ. Physiol.* **301**, H794–H802 (2011).
32. A. C. Rosehart *et al.*, Prostaglandin E(2) dilates intracerebral arterioles when applied to capillaries: Implications for small vessel diseases. *Front. Aging Neurosci.* **13**, 695965 (2021).
33. M. J. Berridge, M. D. Bootman, H. L. Roderick, Calcium signalling: Dynamics, homeostasis and remodelling. *Nat. Rev. Mol. Cell Biol.* **4**, 517–529 (2003).
34. D. E. Clapham, Calcium signaling. *Cell* **131**, 1047–1058 (2007).
35. J. K. Foskett, C. White, K. H. Cheung, D. O. Mak, Inositol trisphosphate receptor Ca2+ release channels. *Physiol. Rev.* **87**, 593–658 (2007).
36. D. C. G. Garcia, T. A. Longden, Ion channels in capillary endothelium. *Curr. Top Membr.* **85**, 261–300 (2020).
37. O. F. Harraz, N. R. Klug, A. J. Senatore, D. C. Hill-Eubanks, M. T. Nelson, Piezo1 is a mechanosensor channel in central nervous system capillaries. *Circ. Res.* **130**, 1531–1546 (2022).
38. B. R. Chen, M. B. Bouchard, A. F. McCaslin, S. A. Burgess, E. M. Hillman, High-speed vascular dynamics of the hemodynamic response. *Neuroimage* **54**, 1021–1030 (2011).
39. C. Iadecola, G. Yang, T. J. Ebner, G. Chen, Local and propagated vascular responses evoked by focal synaptic activity in cerebellar cortex. *J. Neurophysiol.* **78**, 651–659 (1997).
40. R. L. Rungta, E. Chaigneau, B. F. Osmanski, S. Charpak, Vascular compartmentalization of functional hyperemia from the synapse to the pia. *Neuron* **99**, 362–375.e4 (2018).
41. H. Uhlirova *et al.*, Cell type specificity of neurovascular coupling in cerebral cortex. *Elife* **5**, e14315 (2016).
42. C. C. Petersen, A. Grinvald, B. Sakmann, Spatiotemporal dynamics of sensory responses in layer 2/3 of rat barrel cortex measured in vivo by voltage-sensitive dye imaging combined with whole-cell voltage recordings and neuron reconstructions. *J. Neurosci.* **23**, 1298–1309 (2003).
43. J. B. Jensen *et al.*, Biophysical physiology of phosphoinositide rapid dynamics and regulation in living cells. *J. Gen. Physiol.* **154**, e202113074 (2022).
44. B. C. Suh, B. Hille, Recovery from muscarinic modulation of M current channels requires phosphatidylinositol 4,5-bisphosphate synthesis. *Neuron* **35**, 507–520 (2002).
45. D. M. Wu, M. Minami, H. Kawamura, D. G. Puro, Electrotonic transmission within pericyte-containing retinal microvessels. *Microcirculation* **13**, 353–363 (2006).
46. T. Zhang, D. M. Wu, G. Z. Xu, D. G. Puro, The electrotonic architecture of the retinal microvasculature: Modulation by angiotensin II. *J. Physiol.* **589**, 2383–2399 (2011).
47. M. Sancho, N. R. Klug, O. F. Harraz, D. Hill-Eubanks, M. T. Nelson, Distinct potassium channel types in brain capillary pericytes. *Biophys. J.* **123**, 2110–2121 (2024).
48. A. Devor *et al.*, Coupling of total hemoglobin concentration, oxygenation, and neural activity in rat somatosensory cortex. *Neuron* **39**, 353–359 (2003).
49. A. Devor *et al.*, Suppressed neuronal activity and concurrent arteriolar vasoconstriction may explain negative blood oxygenation level-dependent signal. *J. Neurosci.* **27**, 4452–4459 (2007).
50. A. Devor *et al.*, Coupling of the cortical hemodynamic response to cortical and thalamic neuronal activity. *Proc. Natl. Acad. Sci. U.S.A.* **102**, 3822–3827 (2005).